A New Type of Atomic Force Microscope Based On Chaotic Motions

Ming Liu [a,1], David Chelidze [a,*]

[a] *Department of Mechanical Engineering and Applied Mechanics, University of Rhode Island, Kingston, RI, USA*

Abstract

Local flow variation (LFV) method of nonlinear time series analysis is applied to develop a chaotic motion based atomic force microscope (AFM). The method is validated by analyzing time series from a simple numerical model of a tapping mode AFM. For both calibration and measurement procedures the simulated motions of the AFM are nominally chaotic. However, the distance between a tip of the AFM and a sample surface is still measured accurately. The LFV approach is independent of any particular model of the system and is expected to be applicable to other micro-electro-mechanical system sensors where chaotic motions are observed or can be introduced.

Key words: AFM: Atomic Force Microscope, Chaotic Motion, Phase Space Warping, Smooth Orthogonal Decomposition, Local Flow Variation

* Corresponding author.
Email addresses: liumingmech@gmail.com (Ming Liu), chelidze@egr.uri.edu (David Chelidze).
URL: www.mce.uri.edu/chelidze/ (David Chelidze).
[1] Present address: Migma Systems, Inc., 1600 Providence Highway, Walpole, MA

1 Introduction

Atomic-force microscopy (AFM) is a widely used tool for atom level surface analysis. In an AFM, a microscale cantilever with a sharp tip is used to scan the specimen surface, and the vibration of the cantilever is measured to identify the distance between the tip and the specimen surface. Depending on the tip interaction with the specimen surface, an AFM can work in three modes: contact, no contact, and tapping (where the tip oscillates and touches the surface occasionally). Tapping mode AFM is one of the most potent techniques for topographic imaging of substrates. However, data analysis in this mode is prone to complications. In this mode—due to nonlinearities that arise from contact interactions between the tip of a cantilever beam and substrate surface [1]—unwanted dynamic phenomenon such as phase jumps, period doublings, or even chaos are observed [2–6]. These nonlinear effects are difficult to handle using standard data processing and hinder the performance of an AFM system.

To mitigate unwanted dynamical behavior in tapping mode AFM, careful selection of operation parameters and the introduction of various control strategies is the most recommended solution. A large set of parameters, such as driving frequency or stiffness of the cantilever, are available for achieving desired stable periodic motions. However, experimental experience [6,7] shows that the process of finding parameters which ensure stable motions across the whole sample surface is time consuming. In addition, these solutions do not compensate measurement errors caused by the inherent nonlinearity of an AFM.

02081.

Recent work shows that chaotic motions can provide valuable information about system's parameters [8,9], and related nonlinear time series analysis (NTSA) methods have been widely applied [10–12]. Although chaotic motions are observed in different Micro-Electro-Mechanical Systems (MEMS) besides AFM [14], few have attempted to apply these NTSA methods to handle chaotic motions in MEMS [13], and the main reasons are listed as follows: 1) Without setting up a one-to-one relationship between the outcome of NTSA and measurement targets, most of the NTSA methods only provide qualitative results. 2) MEMS work in quite high frequency range (at least several KHz range), and most of the NTSA methods are computationally intensive. Thus, these methods cannot process large amounts of data from MEMS in real time.

In this paper, a new NTSA method, *local flow variation* (LFV) [15], is applied to analyze chaotic motions generated by an AFM system. As a practical implementation of *phase space warping* (PSW) concept [16–19], the LFV provides direct, linear, one-to-one relationship between small changes in system's parameters and LFV-based feature vectors for both chaotic and periodic motions. The LFV is also computationally fast, and can be utilized to process large amount of data generated by MEMS in real time and provide quantitative results.

In this paper, the LFV is applied to analyze signals generated by a numerical model of an AFM. Although the response of the AFM is nominally chaotic, the change of the surface features (distance between the surface and the cantilever tip) is still identifiable. The LFV only assumes that AFM is governed by a deterministic model and its parameters (surface features) change slowly in time. Thus, LFV not only provides an alternative approach to mitigate nonlinear effects widely observed in MEMS, but shows the potential for various

MEMS sensors based on chaotic motions.

In the following section, some basic details of the LFV method are described. Next, a simplified numerical model of and AFM system is introduced, which is used in Section 4, to analyze the chaotic motions generated from the numerical model. The process of AFM sensor calibration and measurement are described next. Finally, the performance of the LFV-based AFM and potential to apply LFV in other MEMS sensors is discussed.

2 Description of the method

This paper follows a basic framework developed for systems with slowly drifting parameters [20]. Specifically, a hierarchical dynamical system is considered where slowly evolving surface features are causing changes in a fast-time AFM system's parameters. Mathematically this can be described as:

$$\dot{\mathbf{x}} = \mathbf{f}(\mathbf{x}, \boldsymbol{\mu}(\boldsymbol{\phi}), t), \quad \dot{\boldsymbol{\phi}} = \epsilon \mathbf{g}(\mathbf{x}, \boldsymbol{\phi}), \quad \text{and} \quad y = h(\mathbf{x}), \tag{1}$$

where overdots denote time (t) differentiation, $\mathbf{x} \in \mathbb{R}^n$ is a fast-time AFM state variable, $\boldsymbol{\phi} \in \mathbb{R}^m$ is a slowly changing surface feature that alters a parameter vector $\boldsymbol{\mu} \in \mathbb{R}^p$, and $y \in \mathbb{R}$ is a measurement taken from the micro-cantilever (usually laser based measurement of the AFM cantilever oscillations). Here, the fast-time is characterized by the time scales associated with the oscillations of the AFM cantilever, and slow-time is characterized by the scan rate of the AFM. In this paper, only topological features of the surface are considered (i.e., $\phi \in \mathbb{R}$). However, in general, the same methodology can be used to identify other surface features, if they affect the fast-time dynamics of the AFM system.

The nonstationary drifts in parameters $\boldsymbol{\mu}$ cause geometric alternations in the phase space of the fast-time AFM system, which are described by the PSW concept [20]. Specifically, the PSW describes the deformation or warping of the phase space trajectories caused by parameter drifts. Recent studies demonstrate that the parameter drifts also influence the probability density or distribution of measured trajectory points in the phase space of the fast-time subsystem [21,22]. So the changes in corresponding statistical moments also reflect parameter variations and can be used as a PSW metrics, which is the basic idea behind the LFV.

In AFM, there is no direct access to the state variable $\mathbf{x}$, only the scalar time series of measurements $\{y_i\}_{i=1}^{N}$ are available. Therefore, instead of working in the true phase space of the AFM system, a reconstructed phase space data is considered $\{\mathbf{y}(i)\}_{i=1}^{N-d+1}$:

$$\mathbf{y}(i) = [y_i, y_{i+\tau}, \ldots, y_{i+(D-1)\tau}]^T \in \mathbb{R}^d, \tag{2}$$

where τ is a delay time and D is an embedding dimension. These *delay coordinate embedding* (DCE) parameters can be determined by standard techniques [23] assuming AFM is a deterministic system. The reconstructed phase space snapshots are obtained from time series recorded over intermediate time periods, over which the drift in parameters can be neglected (the AFM system is assumed to be quasi-stationary over intermediate time scales).

2.1 Local Flow Variation

The LFV characterizes the change in the probability distribution of trajectories in fast-time subsystem's phase space (or the corresponding reconstructed

phase space), which is caused by drifts in the system parameters $\boldsymbol{\mu}$. To quantify the LFV, the first moment of the reconstructed points ($\mathbf{F}_{\mathcal{B}}(\boldsymbol{\phi}) = E_{\mathcal{B}}[\mathbf{y}(n;\boldsymbol{\phi})]$) in a small volume $\mathcal{B}$ of the reconstructed phase space is estimated using:

$$\mathbf{F}_{\mathcal{B}}(\boldsymbol{\phi}) \cong \|\mathcal{B}\|^{-1} \sum_{\mathbf{y}(n;\boldsymbol{\phi})\in\mathcal{B}} \mathbf{y}(n;\boldsymbol{\phi}) \tag{3}$$

where $\mathbf{y}(n;\boldsymbol{\phi}) \in \mathbb{R}^d$ is a sample of the reconstructed fast time trajectory for the current surface parameter $\boldsymbol{\phi}$. It is reasonable to hypothesize that $\mathbf{F}_{\mathcal{B}}(\boldsymbol{\phi})$ is a function of drifting parameter $\boldsymbol{\phi}$ for a given $\mathcal{B}$. Thus, a *LFV tracking function* (FLVTF) is defined as:

$$\mathbf{l}_{\mathcal{B}}(\boldsymbol{\phi}) = \mathbf{F}_{\mathcal{B}}(\boldsymbol{\phi}) - \mathbf{F}_{\mathcal{B}}(\boldsymbol{\phi}_0)\,, \tag{4}$$

where $\boldsymbol{\phi}$ and $\boldsymbol{\phi}_0$ are the current value and reference value of the surface parameters, respectively. If $\mathbf{F}_{\mathcal{B}}(\boldsymbol{\phi})$ is continuous and differentiable, we can expect a *linear observability* of the drifting parameter:

$$\mathbf{l}_{\mathcal{B}}(\boldsymbol{\phi}) = \left.\frac{d\mathbf{F}_{\mathcal{B}}}{d\boldsymbol{\phi}}\right|_{\boldsymbol{\phi}=\boldsymbol{\phi}_0} (\boldsymbol{\phi} - \boldsymbol{\phi}_0) + \mathcal{O}(|\boldsymbol{\phi} - \boldsymbol{\phi}_0|^2). \tag{5}$$

The linear observability is generally expected to hold in the absence of bifurcations in the AFM fast-time dynamics.

Given large amount of data, appropriate choice of the hyper-volume $\mathcal{B}$, and assuming $m < d$, Eq. (5) can be used directly to reconstruct surface features. However, in practice only limited amount of data is available and the optimal choice of hyper-volume is not obvious. In addition, the measurements are usually contaminated by some noise. Therefore, to mitigate all the above mentioned difficulties, the reference reconstructed phase space is partitioned into N_s hyper-cuboids so that each contains approximately the same amount of points. Then, Eq. (5) is evaluated in each of these hyper-cuboids and surface

characteristics (topology, in this case) are inferred by multivariate analysis of the resulting feature vectors. In particular *smooth orthogonal decomposition* (SOD) [20] is used for this purpose.

The LFVTFs are calculated for each small volume $\mathcal{B}_k$ ($k = 1, \ldots, N_s$) reconstructed points from data recorded over intermediate time interval i , and are assembled together into a *feature vector* as:

$$\mathbf{v}_i = [\mathbf{l}_1^i; \mathbf{l}_2^i; ...; \mathbf{l}_{N_s}^i], \tag{6}$$

where $\mathbf{l}_k^i = \mathbf{l}_{\mathcal{B}_k}$ for the data from i-th record, $\mathbf{v}_i \in \mathbb{R}^{d\,N_s}$, and ';' indicates column-wise concatenation of each $\mathbf{l}_k^i$. For further analysis, the feature vectors are assembled in time sequence into a tracking matrix $\mathbf{Y} \in \mathbb{R}^{u \times d\,N_s}$ as row vectors, where u is the total number of data sets recorded over intermediate disjoint time intervals.

2.2 Smooth Orthogonal Decomposition

Given the matrix $\mathbf{Y}$, the SOD is used to identify its linear projection $\boldsymbol{\varphi} = \mathbf{Y}\mathbf{q}$ that maximizes both its smoothness in time and overall variation. The SOD can be described by the following generalized eigenvalue problem:

$$\left[\mathbf{Y}^T\mathbf{Y}\right]\,\mathbf{q} = \lambda\,\left[(\mathbf{D}\mathbf{Y})^T\mathbf{D}\mathbf{Y}\right]\,\mathbf{q}\,, \tag{7}$$

where $\mathbf{D}$ is a differential operator. This type of generalized eigenvalue problem is usually solved by *generalized singular value decomposition* of the matrix pair $[\mathbf{Y}, \mathbf{D}\mathbf{Y}]$ [20].

The idea behind the SOD is that it will find the projections where the local fluctuations in LFVTF due to noise and bifurcations are minimized. The

largest eigenvalue or *smooth orthogonal value* (SOV) λ_1 of the Eq. (7) is associated with the smoothest projection or *smooth orthogonal coordinate* (SOC) φ_1 spanned by the corresponding *smooth orthogonal mode* (SOM) $\mathbf{q}_1$.

In previous studies [19], it was shown that the dominant SOCs can be used to reconstruct slow-time trajectory. In fact, in most of the cases it was shown that there was linear, one-to-one connection between the SOCs $\boldsymbol{\varphi}$ and slow-time variable $\boldsymbol{\phi}$. In this paper, it is expected that the dominating SOC can be used to reconstruct surface topology.

3 Numerical model and its simulation

To illustrate the performance of the LFV-based AFM, a simplified model of an AFM [24]—a nonlinear spring mass system with external excitation (Fig. 1)—is studied:

$$m\ddot{x} + \beta(\dot{x} - \dot{d}) + k(x - d) = f(\delta)\,, \tag{8}$$

where x and d are the displacement of the tip versus the fixed frame and the controller input, respectively; m, β, and k denote the tip mass, damping coefficient, and stiffness coefficient of the spring, respectively. The interaction between the tip and the sample surface is described by the van der Waals attraction/repulsion force $f(\delta)$:

$$f(\delta) = \frac{T}{\delta^2} - \frac{\sigma^6 T}{30\delta^8}\,, \tag{9}$$

where $\delta = z - x$, z is the distance between the fixed frame and the sample surface, σ is the molecular diameter, and T is defined as $T = (A_H R)/6$, A_H is the Hamaker constant, and R denotes the radius of the tip.

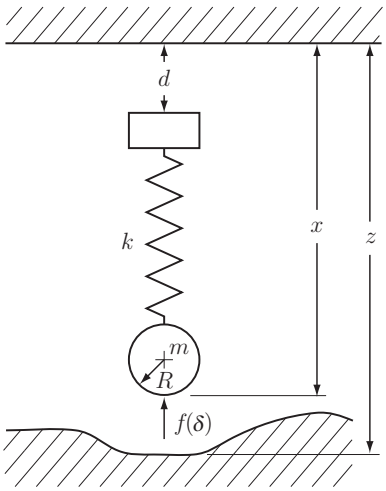

Fig. 1. Simplified model of the AFM system

The system is driven harmonically $d = A\sin(\omega t)$, where A is the driving amplitude and ω is the excitation frequency. The parameters used in the simulation are: $m = 3.1 \times 10^{-7}\,\mathrm{g}$, $k = 0.0167\,\mathrm{N/m}$, $R = 150\,\mathrm{nm}$, $\omega = 8.03 \times 10^{3}\,\mathrm{rad/s}$, $\beta = 0.1$, $A_H = 10^{-19}\,\mathrm{J}$, $\sigma = 3.16 \times 10^{-9}\,\mathrm{m}$, and $A = 2\,\mathrm{nm}$. Scanning processes of the AFM are simulated by changing z. When the tip is close to the sample surface at about 10 nm distance, chaotic motions are observed (see Fig. 2 for an example of the chaotic trajectory of the AFM tip motion). More details about this model and the conditions for chaotic responses are available in [4,25].

4 Calibration and measurement

In simulations, change in the surface topology is simulated by altering z. It is also assumed, that the AFM measurement function is given by $y = h(x) = x$, which is a reasonable assumption, given that laser micrometer measures AFM beam oscillations. Thus, in this paper, x time series need to be used to infer the surface topology z. As every instrument, the chaotic AFM needs to

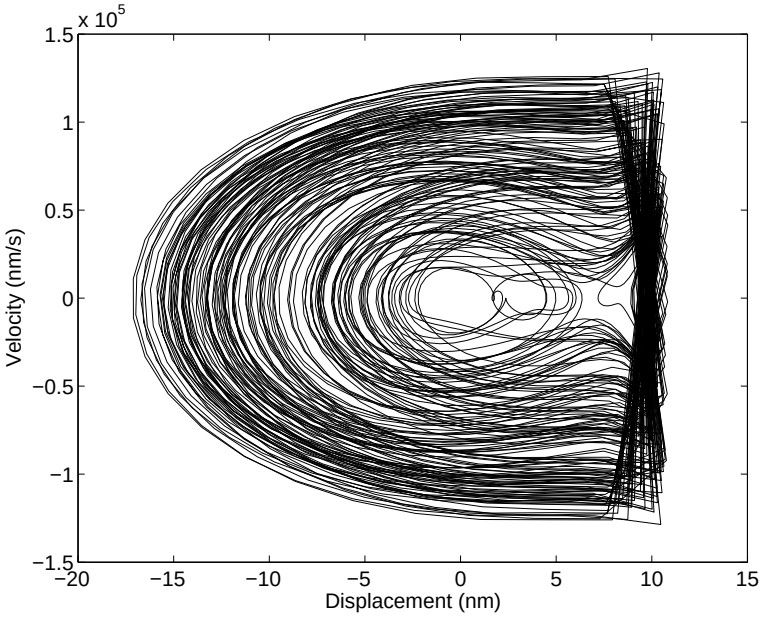

Fig. 2. Phase portrait of the simulated AFM tip motion (x versus $\dot{x}$)

be calibrated. This process is described in the next section, followed by the validation of the measurement procedure.

4.1 Calibration

Since z can be controlled using piezoelectric ceramic transducers in real AFM systems, the calibration approach is straight forward. The distance z is slowly varied in time from 12.23 nm to 12.54 nm as shown in Fig. 3(b). During this process, about 3.4 million data points are collected and are separated into 420 disjoint data sets of 2^{13} points in each. A phase space is reconstructed from each data set using time delay $\tau = 7$ and embedding dimension $D = 5$. The phase space reconstructed for a fixed value of $z = 12.23$ nm is used as a reference phase space. Each of these reconstructions is partitioned into 64 small disjoint hyper-volumes using intervals defined for the three middle coordinates. The partitions are based on a reference phase space data, where the number

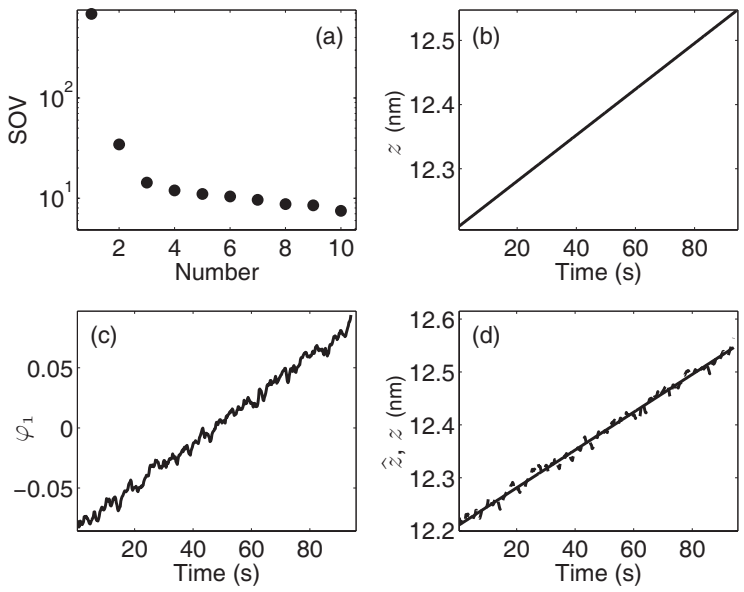

Fig. 3. Calibration using SOD: ten largest SOVs (a); distance between the cantilever tip and the sample surface z versus time (b); identified dominant SOC φ_1 corresponding to the largest SOV λ_1 (c); surface variation z (solid line) and calibrated measurement $\hat{z}$ (dotted line) (d).

of reconstructed trajectory points in each hyper-volume is approximately the same. More details about the partitioning algorithm are available in [18].

The LFV procedure outlined above is used to build a 320×420 tracking matrix $\mathbf{Y}_c$ that characterizes the effects of changing surface topology z. Results of the SOD analysis are depicted in Fig. 3. The largest SOV is much larger than the rest, which means that there is only one smoothly drifting parameter in the system, refer to Fig. 3(a). The corresponding SOC (φ_1) shows a linearly increasing trend similar to z trend as depicted in Fig. 3(b,c)). The best linear fit in the least squares sense is determined to get a calibration function $\hat{z} = a\varphi_1 + b = a\mathbf{Y}\mathbf{q}_1 + b$. From Fig. 3(d), it is clear that $\hat{z}$ tracks z quite well. The resulting calibration parameters ($\mathbf{q}_1$, a, and b) are recorded for future measurements.

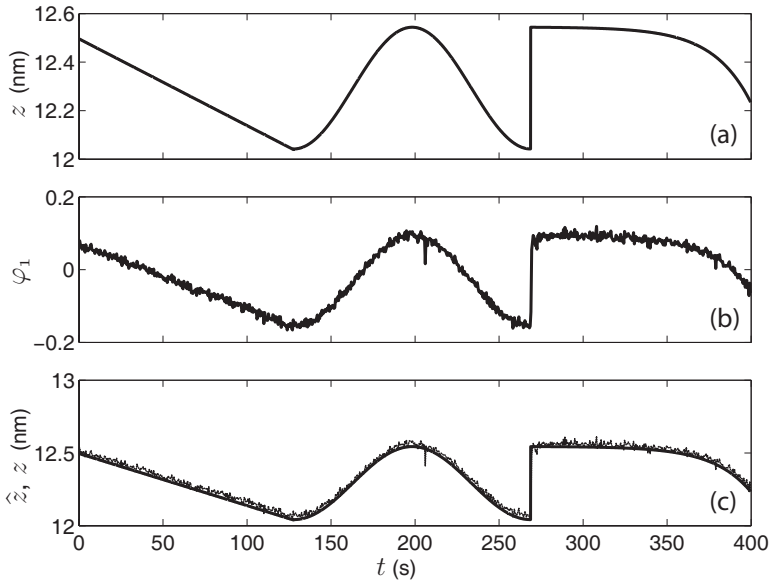

Fig. 4. (a) $z(t)$, distance between the tip and the sample surface; (b) Linear projection of the feature matrix along the SOM from the calibration; (c) $z(t)$ (solid line) and estimated measurement (dotted line).

4.2 Measurement

In practice, changes in surface topology described by z are not expected to be always smooth. However, the calibration parameters allow to track arbitrary small changes in z. For validation purpose, an artificial surface profile z shown in Fig. 4(a) is used for further analysis. 1248 data sets (2^{14} points in each) are collected while varying z according to Fig. 4(a), and a 320×1248 tracking matrix $\mathbf{Y}_m$ is constructed based on LFV procedure. The phase space reconstruction parameters and partitions are exactly the same as for the reference phase space used in the calibration.

Removing DC components from the columns of $\mathbf{Y}_m$ and projecting it along the $\mathbf{q}_1$ SOM identified during the calibration yields the trend φ_1 depicted in Fig. 4(b). Using the calibration function determined *a priori*, $\hat{z} = a\varphi_1 + b$ is plotted in Fig. 4(c), from which it is clear that the $\hat{z}$ tracks the variation in z

quite well, and can be used as its measurement.

5 Discussion

In practice, x variable is not directly measurable, and the AFM oscillations are recorded using a reflection of a laser beam which is projected on the top surface of the cantilever. However, the phase space reconstruction is still expected to work since it only requires that the measurement function $h \in \mathcal{C}^1$, in addition to the fast-time system being deterministic as described in Eq. (1).

In experimental contexts, AFM exhibits chaotic motions in two different tapping modes: (1) "hard tapping" mode, when the equilibrium position of the tip is quite close to the sample surface; and (2) "light tapping" mode, when the tip only touch the sample surface occasionally [26]. In this paper, the simulated AFM system operates in the "hard tapping" mode. This mode is rarely used in practice, since frequent surface touching damages the cantilever tip quickly. However, the LFV methodology does not depend on any specific system model. Thus, similar results are also expected for the "light tapping" mode.

The numerical model considered in this paper is a very simple, one-degree-of-freedom model, where only the first vibration mode of the cantilever beam is considered. In addition, the interaction between the cantilever tip and the sample surface is greatly simplified. Although more sophisticated models are available in literatures [25,27], the use of this simplified model is justified since: (1) the model is able to generate chaotic responses observed in practice; and (2) the LFV methodology does not depend on the specific model. This same

generality can also be exploited in other MEMS sensors where chaotic motions are possible (e.g., a mass sensor, which is chaotically excited).

The performance of the LFV-based AFM is influenced by the size of data sets collected for a given intermediate-size time interval. Generally speaking, the more data is available, the more accurate the tracking result can be. Based on simulation results presented here, it takes 400 s to collect 15 million data points. Since actual AFM systems work in frequencies that are much higher than what is used in the simulation (about 3 Khz), availability of data should not hinder the performance in practical context.

Nominally chaotic motions dominated the data used in this paper. However, due to the bifurcations caused by the parameter drift, periodic and quasi-periodic motion windows were also observed. The SOD is usually capable to filter out bifurcation noise caused by small periodic windows. However, if the periodic window persists over a long time period the quality of measurement may suffer. In the simulation used for this paper, one of the largest periodic bands happened around 210 seconds, which caused unexpected peak in the measurement (see Fig. 4(c)). Thus, it is very important during calibration to identify the suitable range of d and z for which mostly chaotic motions are expected. In addition the simulated time series were noise free, which is impossible in real applications. However, since the LFV relies on the estimated moments of the reconstructed phase space points' probability distribution instead of precise position of individual points, the LFV is still expected to provide reasonable results for noisy signals. The influence of the noise on the performance of the PSW based algorithms is still under investigation.

6 Conclusion

An AFM based on chaotic motion and utilizing LFV methodology was introduced. This methodology is not dependent on particulars of system model and can be easily applied to other MEMS sensors. The basic concepts and procedures were described and a simple one-degree-of-freedom model of the AFM was used to illustrate the calibration and measurement procedures. The calibration process was used to identify range of parameters for which the chaotic response is possible and to find associated calibration parameters. It was demonstrated that chaotic motions can be used to reconstruct the changing topology of a sample surface. Possible complications and corresponding countermeasures were also discussed.

Acknowledgment

This paper is based on the work supported by the NSF CAREER grant No. CMS-0237792.

References

[1] M. Marth, D. Maier, J. Honerkamp, R. Brandsch, G. Bar, A unifying view on some experimental effects in tapping mode atomic force microscopy, Journal of Applied Physics 61 (10) (1999) 4723–4729.

[2] R. Garcia, A. S. Paulo, Attractive and repulsive tip-sample interaction regimes in tapping-mode atomic force microscopy, Physical Review B 60 (7) (1999) 4961–4967.

[3] N. Burnham, A. Kulik, G. Gremaud, G. Briggs, Nanosubharmonics: the dynamics of small nonliner contacts, Physical Review Letters 74 (25) (1995) 5092–5095.

[4] M. Ashhab, M. Salapaka, M. Dahleh, I. Mezic, Dynamical analysis and control of microcantilevers, Automatica 35 (1999) 1663–1670.

[5] M. Basso, L. Giarre, M. Dahleh, I. Mezic, Complex dynamics in a harmonically excited lennard-jones oscillator: microcantilever-sample interaction in scanning probe microscopes, Journal of Dynamic Systems, Measurement, and Control 122 (2000) 240–245.

[6] F. Jamitzky, M. Stark, W. Bunk, W. Heckl, R.W. Stark, Nonlinear dynamics of a microcantilever in close proximity to a surface, in: Proceedings of the IEEE NANO 2004, IEEE, 2004, pp. 38–40.

[7] F. Jamitzky, M. Stark, W. Bunk, W. Heckl, R.W. Stark, Chaos in dynamics atomic force microscopy, Nanotechnology, 17, (2006) 213—220.

[8] S. Guttler, H. Kantz, E. Olbrich, Reconstruction of the parameter spaces of dynamical systems, Physical Review E 63, 056215.

[9] P. F. Verdes, P. M. Granitto, H. D. Navone, H. A. Ceccatto, Nonstationary time series analysis: accurate reconstruction of driving forces, Physical Review Letters 87 (12), 124101.

[10] C. Stam, Nonlinear dynamical analysis of EEG and MEG: Review of an emerging field, Clinical Neurophysiology 116 (2005) 2266–2301.

[11] Y. Diao, G. Feng, S. Liu, S. Liu, D. Luo, S. Huang, W. Lu, J. Chou, Review of the study of nonlinear atmospheric dynamics in china (1999-2002), Advances In Atmospheric Sciences 21 (3) (2004) 399–406.

[12] W. A. Brock, D. A. Hsieh, B. LeBaron, Nonlinear Dynamics, Chaos, and

Instability: Statistical Theory and Economic Evidence, The MIT Press, Cambridge, MA, USA, 1991.

[13] J. Lim, and B.I. Epureanu, Multimode dynamics of atomic-force-microscope tip-sample interactions and application of sensitivity vector fields, Proceedings of the SPIE 6529 (2007) 65293Y.

[14] S. Liu, A. Davidson, Q. Lin, Simulation studies on nonlinear dynamics and chaos in a MEMS cantilever control system, Journal of Micromechanics and Microengineering 14 (2004) 1064–1073.

[15] M. Liu, D. Chelidze, Local flow variation method for damage identification, Smart Materials and Structures 15 (2006) 1830–1836.

[16] D. Chelidze, J. Cusumano, A. Chatterjee, Dynamical systems approach to damage evalution tracking, part I: Desccription and experimental application, Journal of Vibration and Acoutics 124 (2) (2002) 250–257.

[17] D. Chelidze, Identifying multidimensional damage in a hierarchical dynamical system, Nonlinear Dynamics 31 (2004) 307–322.

[18] D. Chelidze, M. Liu, Multidimensional damage identification based on phase space warping: an experimental study, Nonlinear Dynamics 46 (1–2) (2006) 61–72.

[19] D. Chelidze, M. Liu, Dynamical systems approach to fatigue damage identification, Journal of Sound and Vibration 281 (2004) 887–904.

[20] D. Chelidze, W. Zhou, Smooth orthogonal decomposition based modal analysis, Journal of Sound and Vibration 292 (3–5) (2006) 461–473.

[21] L. M. Hively, V. A. Protopopescu, Machine failure forewarning via phase-space dissimilarity measures, Chaos 14 (2) (2004) 408–419.

[22] P. McSharry, L. Smith, L. Tarassenko, Linear and nonlinear methods for automatic seizure detection in scalp electroencephalogram recordings, Medical & Biological Engineering & Computing 40 (4) (2002) 447–461.

[23] H. Kantz, T. Schreiber, Nonlinear Time Series Analysis, 2nd Edition, Cambridge University Press, 2004.

[24] H. N. Pishkenari, N. Jalili, A. Alasty, A. Meghdari, Nonlinear dynamic analysis and chaotic behavior in atomic force microscopy, in: IDETC/CIE 2005, ASME, 2005, pp. 1–3.

[25] N. Jalili, A fresh insight into the microcantilever-sample interaction problem in non-contact atomic force microscopy, Journal of Dynamic Systems, Measurement, and Control 126 (2004) 327–335.

[26] S. Hu, A. Raman, Chaos in atomic force microscopy, Physical Review Letters 96 (3), 036107.

[27] S. Lee, S. Howell, A. Raman, R. Reifenberger, C. Nguyen, M. Meyyappan, Complex dynamics of carbon nanotube probe tips, Ultramicroscopy 103 (2005) 95–102.